Monthly Notices
of the
ROYAL ASTRONOMICAL SOCIETY

MNRAS **500,** L27–L31 (2021)
Advance Access publication 2020 October 27

doi:10.1093/mnrasl/slaa176

Physical explanation for the galaxy distribution on the (λ_R, ε) and (V/σ, ε) diagrams or for the limit on orbital anisotropy

Bitao Wang [1,2,3]★ Michele Cappellari [3] and Yingjie Peng [2]★

[1] *Department of Astronomy, School of Physics, Peking University, Beijing 100871, China*
[2] *Kavli Institute for Astronomy and Astrophysics, Peking University, Beijing 100871, China*
[3] *Sub-department of Astrophysics, Department of Physics, University of Oxford, Denys Wilkinson Building, Keble Road, Oxford OX1 3RH, UK*

Accepted 2020 October 14. Received 2020 September 18; in original form 2020 May 29

ABSTRACT

In the (λ_R, ε) and (V/σ, ε) diagrams for characterizing dynamical states, the fast-rotator galaxies (both early type and spirals) are distributed within a well-defined leaf-shaped envelope. This was explained as due to an upper limit to the orbital anisotropy increasing with galaxy intrinsic flattening. However, a physical explanation for this empirical trend was missing. Here, we construct Jeans Anisotropic Models (JAM), with either cylindrically or spherically aligned velocity ellipsoid (two extreme assumptions), and each with either spatially constant or variable anisotropy. We use JAM to build mock samples of axisymmetric galaxies, assuming on average an oblate shape for the velocity ellipsoid (as required to reproduce the rotation of real galaxies), and limiting the radial anisotropy β to the range allowed by physical solutions. We find that all four mock samples naturally *predict* the observed galaxy distribution on the (λ_R, ε) and (V/σ, ε) diagrams, without further assumptions. Given the similarity of the results from quite different models, we conclude that the empirical anisotropy upper limit in real galaxies, and the corresponding observed distributions in the (λ_R, ε) and (V/σ, ε) diagrams, are due to the lack of physical axisymmetric equilibrium solutions at high β anisotropy when the velocity ellipsoid is close to oblate.

Key words: galaxies: evolution – galaxies: formation – galaxies: kinematics and dynamics – galaxies: structure.

1 INTRODUCTION

Gravitation dominates in galaxies and makes thermal equilibrium unattainable, so that their current configurations cannot be simply explained as states of maximum entropy (e.g. Binney & Tremaine 2008). To understand the present states of galaxies, it requires the knowledge about the initial conditions of their formation and the subsequent dynamical processes they experienced. Important clues to the assembly histories can be held in stellar kinematics (e.g. review by Cappellari 2016).

One way to characterize the stellar kinematics is the anisotropy of the orbital distribution quantified through the ratio of orthogonal velocity dispersions. Decades ago, elliptical galaxies were thought to be isotropic and flattened by rotation (e.g. Gott 1975). However, long-slit spectra of bright elliptical galaxies revealed too low rotation velocities against their presumed isotropy (Bertola & Capaccioli 1975; Illingworth 1977; Binney 1978). Orbital anisotropy was proposed to explain the low levels of rotation observed at different galaxy shapes (Binney 1976, 1978). Following works were extended on to small samples of fainter ellipticals (Davies et al. 1983) and bulges of spiral galaxies (Kormendy 1982; Kormendy & Illingworth 1982) that showed that most of them had rotation comparable to isotropic rotators. While more recent works also indicated the existence of fainter early-type galaxies (ETGs) with significant anisotropy (Cappellari et al. 2007; Thomas et al. 2009).

Using three-integral axisymmetric toy models, Thomas et al. (2009) shows that at fixed flattening galaxies achieve higher entropy with larger velocity anisotropy. Therefore, perturbations that move galaxies away from equilibrium may lead to configurations of larger anisotropy. Structures on the discs such as giant molecular clouds, bars, and spiral arms can perturb stars and heat them anisotropically (Spitzer & Schwarzschild 1951; Jenkins & Binney 1990; Shapiro, Gerssen & van der Marel 2003). Mergers may enhance the vertical velocity dispersion relative to the dispersions on equatorial plane (Toth & Ostriker 1992; Benson et al. 2004). Thob et al. (2019) reports that the anisotropy also correlates with the intrinsic shapes of inner dark matter haloes.

Based on tensor virial theorem, for a given intrinsic ellipticity galaxies can display any bulk rotation velocity between a maximum value and no rotation at all (Binney 2005). Lower rotations can be achieved by increasing the anisotropy up to a maximum theoretical value at $V/\sigma = 0$. However, the first statistically significant set of three-integral axisymmetric Schwarzschild (1979) models of galaxies based on integral-field stellar kinematics revealed that real galaxies do not reach the maximum anisotropy allowed by the tensor virial theorem, but instead lie below a limit $\beta \lesssim 0.7 \times \varepsilon_{\rm intr}$ (the 'magenta line' of Cappellari et al. 2007). This upper limit appeared consistent with the observed lower boundary of the distribution of fast rotators on the (V/σ, ε) diagram.

The distribution of galaxy samples with ever-increasing size (Emsellem et al. 2011; Graham et al. 2018; Wang et al. 2020) on either the (V/σ, ε) diagram by Binney (2005) or the (λ_R, ε) diagram by Emsellem et al. (2007), unambiguously confirmed that galaxies

★ E-mail: bt-wang@pku.edu.cn (BW); yjpeng@pku.edu.cn (YP)

follow the leaf-like distribution predicted by randomly oriented axisymmetric models with anisotropy upper limit that increases with their intrinsic flattening (section 3 in the review by Cappellari 2016). However, a physical explanation for the existence of this empirical relation between anisotropy and shape was not known and we try to find it in this Letter by exploiting Jeans Anisotropic Models (JAM) of galaxy dynamics.

2 DATA AND MODELS

The dynamic models used in this work are solutions for steady-state axisymmetric Jeans equations of velocity second moments (Jeans 1922), allowing for velocity anisotropy. Specifically, the equation solutions[1] based on the Multi-Gaussian Expansion (MGE; Emsellem, Monnet & Bacon 1994; Cappellari 2002) formalism are given in Cappellari (2008, 2020) making the two extreme assumptions of a cylindrically aligned ($\mathrm{JAM_{cyl}}$) and a spherically aligned ($\mathrm{JAM_{sph}}$) velocity ellipsoid, respectively. The two models with different velocity ellipsoid alignment are characterized by anisotropy parameters of orthogonal velocity dispersions (Binney & Mamon 1982; Binney & Tremaine 2008):

$$\beta_{\rm cyl}(R,z) \equiv 1-(\sigma_z/\sigma_R)^2 \qquad \beta_{\rm sph}(r,\theta) \equiv 1-(\sigma_\theta/\sigma_r)^2, \tag{1}$$

$$\gamma_{\rm cyl}(R,z) \equiv 1-(\sigma_\phi/\sigma_R)^2 \qquad \gamma_{\rm sph}(r,\theta) \equiv 1-(\sigma_\phi/\sigma_r)^2. \tag{2}$$

We assume spatially constant total mass-to-light ratio (M/L), which is approximate. But even accounting for stellar-M/L gradients and the dark matter, within one half-light radius ($R_{\rm e}$) where our measurements will be carried out, the profiles of total mass indeed closely follow those of the stellar mass (e.g. fig. 10 of Poci, Cappellari & McDermid 2017). This explains the success of the mass-follow-light models in describing the integral-field kinematics of real galaxies (Cappellari et al. 2013). The contribution of central supermassive black holes is ignored due to its minimal influence on the kinematics of the scale that we are interested in.

We build dynamic models based on realistic galaxy light distributions. The MGE photometric models of *r*-band light of 112 regular-rotator ATLAS$^{\rm 3D}$ ETGs are taken from Scott et al. (2013). This is a subsample of the 260 ATLAS$^{\rm 3D}$ ETGs and includes all fast rotators (as flagged 'F' in table B1 by Emsellem et al. 2011) with high inclination ($i > 60^\circ$). The inclination was measured via JAM dynamic modelling and taken from table 1 of Cappellari et al. (2013), including only reliable measurements ('quality' >0). This inclination criterion is meant to reduce the uncertainty in the mass-deprojection degeneracy (Rybicki 1987), crucial for deriving the intrinsic density profiles of galaxies. The focus of this study is the leaf-like envelope of the fast rotators. So, we exclude slow rotators as they are generally triaxial (Cappellari 2016) and do not follow the distribution of the fast rotators. And reproducing the envelope requires adequate coverage of intrinsic ellipticities of the real galaxies that form the envelope, which is satisfied by our sample.

For a direct comparison with observation, we measure ellipticity, $(V/\sigma)_{\rm e}$ and $\lambda_{R_{\rm e}}$ as is done for real galaxies using integral-field data. The effective ellipticity ε and $(V/\sigma)_{\rm e}$ are measured within the half-light isophote as defined in equations (10)–(11) of Cappellari et al. (2007). This ellipticity is measured from the MGE parametrization of the surface brightness with the routine MGE_HALF_LIGHT_ISOPHOTE[2]

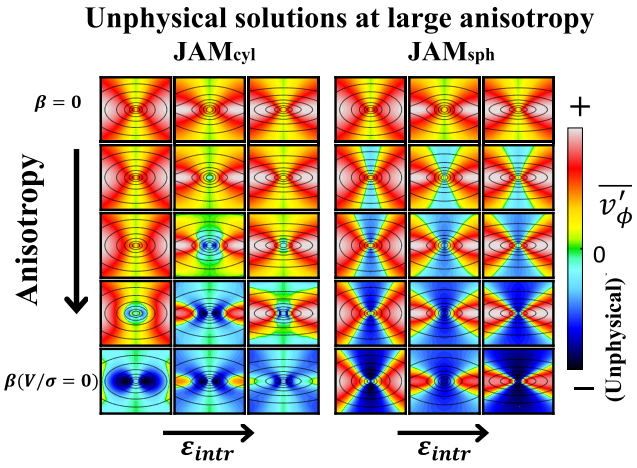

Figure 1. $\overline{v'_\phi}(R,z) = \mathrm{sign}(\overline{v_\phi}^2) \times |\overline{v_\phi}^2|^{1/2}$ maps derived with $\mathrm{JAM_{cyl}}$ (left-hand panels) and $\mathrm{JAM_{sph}}$ (right-hand panels) for three galaxies with $\varepsilon_{\rm intr}$ increasing from left to right (NGC 4551, NGC 4474, and NGC 0448). β increases from zero to the maximum value allowed by tensor virial theorem for certain $\varepsilon_{\rm intr}$. In each panel, the overlaid black lines show the density contours.

that implements the steps (i)–(iv) above equation (12) in Cappellari et al. (2013). The specific angular momentum proxy $\lambda_{R_{\rm e}}$ is computed as defined in equations (1)–(2) of Emsellem et al. (2007).

3 NON-PHYSICAL MODELS AT LARGE ANISOTROPY

Cappellari et al. (2007) found that real galaxies have $\gamma_{\rm cyl}$ around zero and the main trend of anisotropy with flattening is driven by the systematic change of $\beta_{\rm cyl}$. This on-average oblate shape (i.e. $\sigma_\phi \sim \sigma_R$) of the velocity ellipsoid in fast-rotator ETGs is strikingly apparent in fig. 11 of Cappellari (2016).

If one fixes γ and increases β, the models become unphysical when the *squared* streaming velocities $\overline{v_\phi}^2 = \overline{v_\phi^2} - \sigma_\phi^2$ is significantly negative in non-negligible parts of the models. Examples are given in Fig. 1 that shows maps[3] of $\overline{v'_\phi}(R,z) \equiv \mathrm{sign}(\overline{v_\phi}^2) \times |\overline{v_\phi}^2|^{1/2}$ in a $1R_e \times 1R_e$ region and in a (R,z,ϕ) cylindrical coordinate system where the z axis is the galaxy symmetry axis. For each galaxy, β increases with a certain linear step from $\beta = 0$ at the top panel to the maximum anisotropy allowed by the tensor virial theorem $\beta(V/\sigma = 0)$ at the bottom. The colour bar range of $\overline{v'_\phi}$ is symmetric about zero so that unphysical areas have blue colours. Note that unphysical models are expected as the Jeans equations themselves do not guarantee physically meaningful solutions.

Isotropic models (the first row) are entirely physical with non-negative values of $\overline{v'_\phi}$ everywhere. At certain large values of β, parts of the models start having significantly negative (dark blue) $\overline{v'_\phi}$. These unphysical regions grow with further increased β. The anisotropy at which a model becomes mildly unphysical can be considered as a natural upper limit for β.

[1] We used v6.2 of the JAMPY PYTHON software package available from https://pypi.org/project/jampy/.
[2] Also included in the JAMPY PYTHON software package.
[3] For $\overline{v_\phi}^2 > 0$, the $\overline{v'_\phi}$ is the usual streaming velocity, while for $\overline{v_\phi}^2 < 0$, the $\overline{v'_\phi}$ is the absolute value of the complex $\overline{v_\phi}$, but we give it a negative sign to indicate it is unphysical.

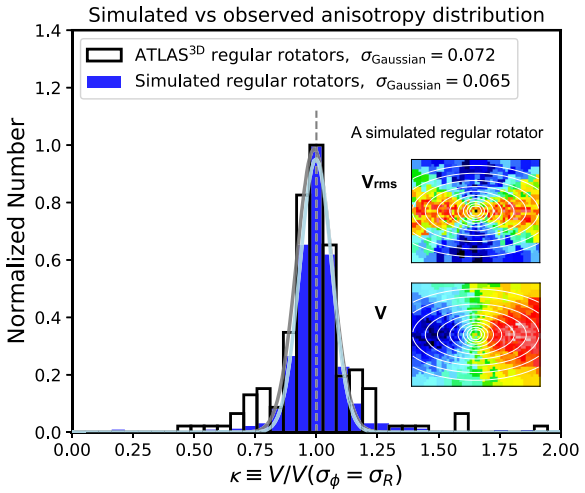

Figure 2. The consistency in the anisotropy κ distributions of simulated regular rotators (blue) under our assumed γ distribution and the ATLAS^{3D} regular rotators (white). The histograms are normalized by the peaks and the light blue and grey curves are the best-fitting Gaussians for the simulation and observation, respectively. The velocity and root-mean-square velocity of a projected regular rotator are shown as an example of the mock data.

4 PREDICTED (V/σ, ε) AND (λ_R, ε) DISTRIBUTIONS

We carry out Monte Carlo simulations to model the distribution of galaxies on the (β, $\varepsilon_{\rm intr}$), (λ_R, ε), and (V/σ, ε) diagrams similar to what was done in appendix C of Cappellari et al. (2007) or appendix B of Emsellem et al. (2011). The key difference, and the novelty of this paper, is that in our case the anisotropy β of each galaxy is not assumed but comes directly from the requirement of a physical JAM solution for each galaxy.

4.1 Modelling the tangential anisotropy

A crucial aspect of our simulations is the choice for the distribution of tangential anisotropy γ. It is clear that one can construct physical axisymmetric galaxy models with arbitrarily low level of V/σ or λ_R by allowing for counter-rotating discs (section 3.4.3 of Cappellari 2016) that have large γ and fall well below the leaf-like envelope populated by fast rotators. However, observationally counter-rotating discs are rare and the area below the leaf-like envelope in the (V/σ, ε) and (λ_R, ε) diagrams is sparsely populated.

To make sure that our mock galaxies match the γ anisotropy of real galaxies, we require them to reproduce both (i) the measured range of γ for fast rotators, from Schwarzschild models, in fig. 2 of Cappellari et al. (2007) and (ii) the distribution of rotation parameter κ, from Jeans models, in fig. 11 of Cappellari (2016). Here, κ is defined by equation (52) in Cappellari (2008) as the ratio of observed rotation and the rotation of a model with oblate velocity ellipsoid, and can be considered as a quantification of the tangential anisotropy.

Closely mimicking the observation, in our simulations each projected model (described in Section 4.2) is spatially Voronoi binned (Cappellari & Copin 2003) and Gaussian noises with dispersions $\varepsilon_V = 0.1V_{\rm max}$ and $\varepsilon_\sigma = 0.1\sigma$ are added to the kinematics, producing realistic maps (see an example in Fig. 2). The JAM$_{\rm cyl}$ models are then treated as mock observations by first fitting the $V_{\rm rms}$ for β, inclination and M/L and then fitting the V for κ.

We found that we can reproduce the above two anisotropy observations by adopting a Gaussian distribution for the ratio σ_ϕ/σ_R with mean $\mu = 1$ and dispersion $\sigma = 0.07$. This results in a γ distribution with tails extending to $\gamma \approx \pm 0.2$, consistent with Cappellari et al. (2007), and a distribution of κ that quantitatively matches the observations (Fig. 2).

4.2 Models with spatially constant anisotropy

For each galaxy in our sample, we compute 10 models based on its deprojected MGE density distribution. This is done separately for both the JAM$_{\rm cyl}$ and the JAM$_{\rm sph}$ models with the intrinsic kinematics computed with the procedure JAM_AXI_INTR, using the keyword `align='cyl'` and `align='sph'` respectively.

For every model, we start by drawing a value of the ratio σ_ϕ/σ_R for JAM$_{\rm cyl}$ (or σ_ϕ/σ_r for JAM$_{\rm sph}$) from the Gaussian distribution determined in Section 4.1. With this sampled γ, then we try a sequence of β values starting from 0 and increasing with a step 0.02, to find out at which value the model meets our 'mildly unphysical' criterion. We have tried a variety of slightly different 'mildly unphysical' criteria: (i) $|\min(\overline{v'_\phi})| > f_1 \times \max(\overline{v'_\phi})$ (the peak unphysical velocity is no longer small compared with the physical one); (ii) $f_{V_{\rm neg}} > f_2$ (the volume fraction of unphysical part of the model is no longer small); (iii) the two criteria combined, where f_1 and f_2 are constants; or (iv) the fraction of volume where $|\min(\overline{v'_\phi})| > f_1 \times \max(\overline{v'_\phi})$ is larger than f_2. And for direct comparison with observation, we only take into account the part of the model enclosed within the half-light ellipse in the (R, z) plane. We obtained qualitatively similar results with all these different criteria, but in the following, we adopted the first one (i) as our standard criterion with $f_1 = 0.2$. This criterion typically corresponds to an unphysical volume fraction of several per cent inside the half-light ellipse, which indeed indicates an at most mildly unphysical model.

Given that nearly every physical model is only a simplified version of reality, it does not make sense to define the model as unphysical as soon as the first values of $\overline{v_\phi}^2$ become negative. This would lead to an unrealistically too strict criterion, as we try to qualitatively approximate what may happen in real galaxies and are not interested in the mathematical aspects of the JAM solutions.

After finding the upper limit $\beta_{\rm ul}$, for the model we uniformly sample a value for β in the range [0, $\beta_{\rm ul}$]. This assumes that real galaxies can possess the full range of anisotropy allowed by physical solutions. Biasing the sampling towards low or high anisotropy gives qualitatively the same results. Lastly, we draw a random orientation on the sphere of viewing angles. We use the JAM procedure JAM_AXI_PROJ to compute the predicted kinematics projected along the line of sight, out of which we measure $(V/\sigma)_{\rm e}$ and $\lambda_{R_{\rm e}}$ using the standard approach as used in observation. Note that, during the line-of-sight integration, the JAM_AXI_PROJ procedure sets $\overline{v_\phi} = 0$ to the unphysical part. This makes little difference to the projected kinematics, given that we only consider mildly unphysical models and the volume fraction of the unphysical part is typically only several percent inside $R_{\rm e}$.

The two left-hand panels of Fig. 3 show the final distribution of $\beta_{\rm ul}$ as a function of $\varepsilon_{\rm intr}$ for JAM$_{\rm cyl}$ and JAM$_{\rm sph}$, respectively. In the panels, the magenta line ($\beta = 0.7\varepsilon_{\rm intr}$) is the empirical upper limit based on both the Schwarzschild models of Cappellari et al. (2007) and the Jeans models of Cappellari et al. (2013), while the black-dashed line is the zero rotation limit set by tensor virial theorem when $\gamma = 0$.

The results indicate that the magenta line approximately corresponds to the upper limit for the JAM models under the condition of being physical. The tolerance of velocity anisotropy varies

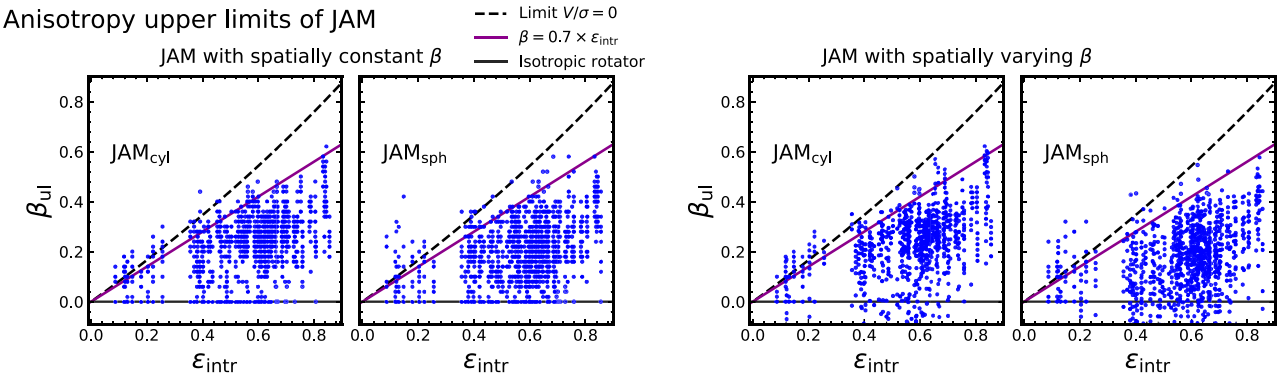

Figure 3. Anisotropy upper limit $\beta_{\rm ul}$ as a function of intrinsic ellipticity $\varepsilon_{\rm intr}$ of JAM models assuming spatially constant β (left-hand panels) and spatially varying β (right-hand panels). In each case, cylindrically and spherically aligned velocity ellipsoids are assumed, respectively. $\beta_{\rm ul}$ is the anisotropy from where the model (based on the density profile of a certain galaxy) is considered mildly unphysical and thus unrepresentative for real galaxies. For the models with spatially varying β, $\beta_{\rm ul}$ is integrated within the half-light ellipse. The upper bound of $\beta_{\rm ul}$ in each panel roughly matches the magenta line, an empirical upper limit from Cappellari et al. (2007), and is below the maximum allowed by tensor virial theorem under $\gamma = 0$ (the black-dashed line).

significantly between different galaxy density profiles and only some of them have $\beta_{\rm ul}$ close to the magenta line.

The distributions of projected models on $(V/\sigma,\ \varepsilon)$ and $(\lambda_{\rm R},\ \varepsilon)$ planes are shown in the four left-hand panels of Fig. 4. Under the conditions $\beta = 0.7\varepsilon_{\rm intr}$ and $\gamma = 0$, the edge-on prediction (the solid magenta line in Fig. 4) from tensor virial theorem together with its projections at different inclinations (the magenta dashed and dotted lines) form the envelope (the 'magenta leaf' of Cappellari et al. 2007) that matches well the observed distribution boundaries of ATLAS$^{\rm 3D}$ (Emsellem et al. 2007), MaNGA (Graham et al. 2018), and SAMI (van de Sande et al. 2017) galaxies (see more about the theoretical tracks in section 3.5 of Cappellari 2016).

The resultant distributions of $\rm JAM_{cyl}$ models in the first column highly resemble the ones of real galaxies that are represented by the magenta envelopes. A similarity between observations and models is also visible in the second column for $\rm JAM_{sph}$ models, but to a lesser degree. This may imply that the velocity ellipsoid of real galaxies is on average better described by cylindrically than spherically aligned models.

4.3 Models with spatially variable anisotropy

While a spatially constant anisotropy β is assumed previously, in real galaxies β can vary with spatial position. However, there are no systematic analyses of the anisotropy variation in fast rotators. Studies of a handful of galaxies with high-quality integral-field stellar kinematics have found that, beyond the sphere of influence of the central supermassive black hole, the σ_z/σ_R ratio varies on the order of 20 per cent within $R_{\rm e}$ (e.g. Cappellari et al. 2008; Krajnović et al. 2018).

To model the β variation, we assume that the rounder bulges and stellar haloes are more isotropic than the discs. And in the previous Monte Carlo simulation, while searching for $\beta_{\rm ul}$ we multiply the dispersion ratio (e.g. σ_z/σ_R for $\rm JAM_{cyl}$) by a factor of 1.1 for the inner or rounder MGE components (the Gaussians with $\sigma < 0.3R_{\rm e}$ or axial ratio $q > 0.7$) and a factor of 1/1.1 for the remaining flatter and outer components. The typical change of β is then $\sim$0.2 inside one $R_{\rm e}$, increasing outwards. When the mildly unphysical criterion is met, we record the flux-weighted β inside one $R_{\rm e}$ as $\beta_{\rm ul}$. The results under spatially varying β are shown in the right-hand panels of Figs 3 and 4. No significant difference is seen compared with the results under spatially constant β.

5 CONCLUSIONS

In this letter, we have used Jeans anisotropic models in combination with realistic stellar density distributions of ATLAS$^{\rm 3D}$ galaxies to try to understand the physical origin for the observed distribution of fast-rotator galaxies (spirals and ETGs) on both the $(\lambda_{\rm R_e},\ \varepsilon)$ and the $[(V/\sigma)_e,\ \varepsilon]$ diagrams, and for the empirical upper limit on the radial anisotropy β as a function of the galaxy intrinsic flattening.

We found that if we adopt an on-average oblate velocity ellipsoid, as constrained by the observations, and require our models to be no more than mildly unphysical (i.e. at most having only weakly negative $\overline{v_\phi}^2$), and randomly project the models on the plane of the sky, we can naturally reproduce the observed distributions of galaxies without the need to make additional assumptions about the galaxy anisotropy. This is true for two extreme assumptions on the orientation of the velocity ellipsoid (either cylindrically or spherically aligned) and for both spatially constant and variable anisotropy. The result remains qualitatively similar for different criteria to define an unphysical model.

Although our models only approximately describe real galaxies, the robustness of the qualitative result against the different assumptions suggests that the same general phenomenon may apply to real galaxies. We conclude that the leaf-like distribution of galaxies on the $(\lambda_{\rm R_e},\ \varepsilon)$ and the $[(V/\sigma)_e,\ \varepsilon]$ diagrams, as well as the empirical upper limit on the radial anisotropy β, are due to the lack of physical equilibrium solutions at large β among regular rotators. The only way that fast-rotator galaxies appear to reach the lowest levels of rotation is when the galaxies contain counterrotating discs, which are rare in the general population.

ACKNOWLEDGEMENTS

We thank our referee for the thoughtful comments. BW acknowledges the financial support from the China Scholarship Council during his stay in Oxford. YP acknowledges the National Key Research and Development Program of China, Grant 2016YFA0400702 and NSFC Grants 11773001, 11721303, and 11991052.

DATA AVAILABILITY

The MGE photometric models used in this work are available from https://purl.org/atlas3d

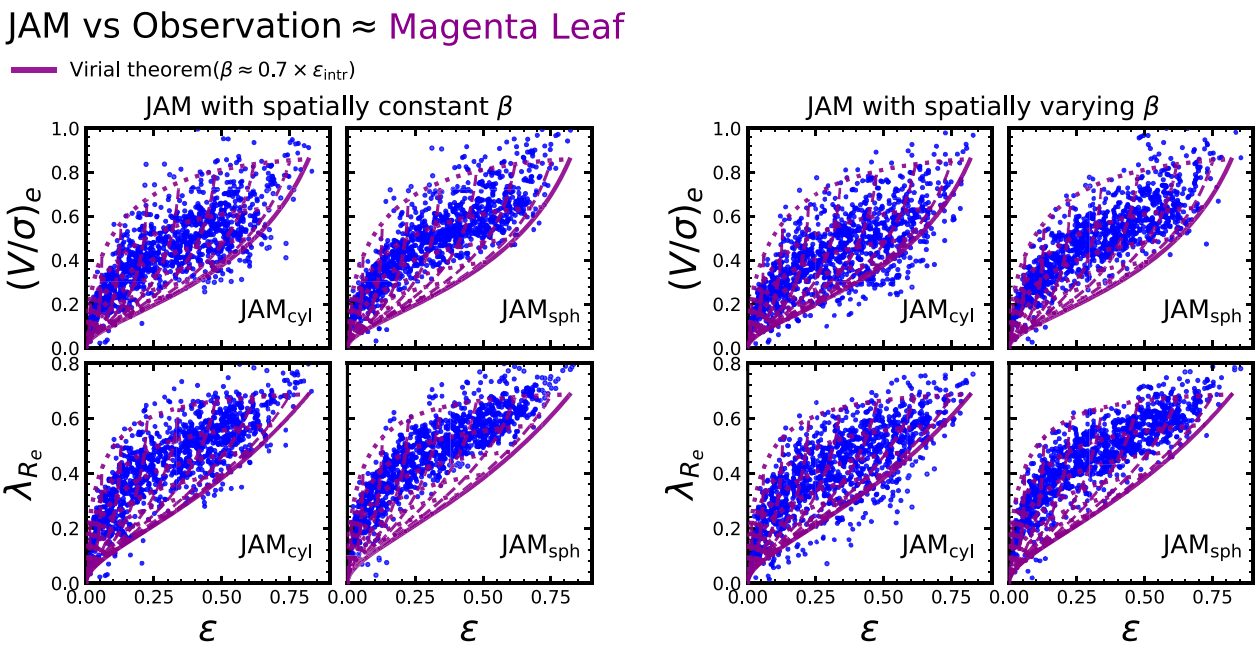

Figure 4. $(V/\sigma)_{\rm e}$ (upper row) and $\lambda_{R_{\rm e}}$ (lower row) as a function of ellipticity ε for JAM models projected at random inclinations, assuming spatially constant β (left-hand panels) and spatially varying β (right-hand panels). Again, in each case cylindrically and spherically aligned velocity ellipsoids are assumed, respectively. Anisotropy β of each model is restricted by the physical upper limit $\beta_{\rm ul}$ that is determined, respectively, for each model. Virial theorem predictions for oblate rotators following the anisotropy relation $\beta \approx \delta = 0.7 \times \varepsilon_{\rm intr}$ of Cappellari et al. (2007) are shown, with the solid magenta line showing an edge-on view at different intrinsic ellipticities, and the dotted and dashed magenta lines for other inclinations. Note that this 'magenta leaf' envelope approximately covers the area populated by real galaxies in this $\varepsilon_{\rm intr}$ range.

REFERENCES

Benson A. J., Lacey C. G., Frenk C. S., Baugh C. M., Cole S., 2004, MNRAS, 351, 1215
Bertola F., Capaccioli M., 1975, ApJ, 200, 439
Binney J., 1976, MNRAS, 177, 19
Binney J., 1978, MNRAS, 183, 501
Binney J., 2005, MNRAS, 363, 937
Binney J., Mamon G. A., 1982, MNRAS, 200, 361
Binney J., Tremaine S., 2008, Galactic Dynamics, 2nd edn. Princeton Univ. Press, Princeton, NJ
Cappellari M., 2002, MNRAS, 333, 400
Cappellari M., 2008, MNRAS, 390, 71
Cappellari M., 2016, ARA&A, 54, 597
Cappellari M., 2020, MNRAS, 494, 4819
Cappellari M., Copin Y., 2003, MNRAS, 342, 345
Cappellari M. et al., 2007, MNRAS, 379, 418
Cappellari M. et al., 2008, in Bureau M., Athanassoula E., Barbuy B., eds, Proc. IAU Symp. 245, Formation and Evolution of Galaxy Bulges. Kluwer, Dordrecht, p. 215
Cappellari M. et al., 2013, MNRAS, 432, 1709
Davies R. L., Efstathiou G., Fall S. M., Illingworth G., Schechter P. L., 1983, ApJ, 266, 41
Emsellem E. et al., 2007, MNRAS, 379, 401
Emsellem E. et al., 2011, MNRAS, 414, 888
Emsellem E., Monnet G., Bacon R., 1994, A&A, 285, 723
Gott J. Richard I., 1975, ApJ, 201, 296
Graham M. T. et al., 2018, MNRAS, 477, 4711
Illingworth G., 1977, ApJ, 218, L43
Jeans J. H., 1922, MNRAS, 82, 122
Jenkins A., Binney J., 1990, MNRAS, 245, 305
Kormendy J., 1982, ApJ, 257, 75
Kormendy J., Illingworth G., 1982, ApJ, 256, 460
Krajnović D. et al., 2018, MNRAS, 477, 3030
Poci A., Cappellari M., McDermid R. M., 2017, MNRAS, 467, 1397
Rybicki G. B., 1987, in de Zeeuw P. T., ed., Proc. IAU Symp. 127, Structure and Dynamics of Elliptical Galaxies. Reidel, Dordrecht, p. 397
Schwarzschild M., 1979, ApJ, 232, 236
Scott N. et al., 2013, MNRAS, 432, 1894
Shapiro K. L., Gerssen J., van der Marel R. P., 2003, AJ, 126, 2707
Spitzer Lyman J., Schwarzschild M., 1951, ApJ, 114, 385
Thob A. C. R. et al., 2019, MNRAS, 485, 972
Thomas J. et al., 2009, MNRAS, 393, 641
Toth G., Ostriker J. P., 1992, ApJ, 389, 5
van de Sande J. et al., 2017, ApJ, 835, 104
Wang B., Cappellari M., Peng Y., Graham M., 2020, MNRAS, 495, 1958

This paper has been typeset from a TEX/LATEX file prepared by the author.